Phys. Status Solidi B **247**, Nos. 11–12, 2768–2773 (2010) / **DOI** 10.1002/pssb.201000350

physica status solidi b
www.pss-b.com
basic solid state physics

Revealing new electronic behaviours in the Raman spectra of chirality-enriched carbon nanotube ensembles

Juan G. Duque[1], Hang Chen[2], Anna K. Swan[2], Erik H. Hároz[3], Junichiro Kono[3], Xiaomin Tu[4], Ming Zheng[4], and Stephen K. Doorn[*,1]

[1] Center for Integrated Nanotechnologies, Los Alamos National Laboratory, MS-K771, Los Alamos, NM 87545, USA
[2] Department of Electrical and Computer Engineering, Boston University, Boston, MA 02215, USA
[3] Department of Electrical and Computer Engineering, Rice University, PO Box 1892, MS-366, Houston, TX 77005, USA
[4] Polymer Division, National Institute of Standards and Technology, 100 Bureau Dr., Stop 8540, Gaithersburg, MD 20899-8540, USA

Received 21 May 2010, accepted 14 July 2010
Published online 13 September 2010

Keywords carbon nanotube, G band, Raman, resonance profile, separations

[*] Corresponding author: e-mail skdoorn@lanl.gov, Phone: 505 667 2541, Fax: 505 665 9030

We present Raman spectroscopy of single-walled carbon nanotubes (SWNTs) that are enriched in metallic species by density gradient ultracentrifugation (DGU) and enriched in single semiconducting chiralities through DNA-based separations. Radial breathing mode (RBM) spectra demonstrate that DGU samples are highly enriched in armchair chiralities. The enrichment allows acquisition of pure G-band spectra of the armchair SWNTs and reveals that the LO mode is absent in these structures. Raman excitation profiles for the G-band in nearly pure (10,2) samples reveals a strong asymmetry in the intensities of the resonance coupling to incident and scattered photons. The experimental data may be fit using a four-level molecular model for Raman scattering and the strong asymmetry can be understood as a consequence of the presence of non-Condon effects. The result requires a reassessment of the assumption that the incident and scattered resonances are equivalent. The consequences of such non-Condon effects on other SWNT electronic and optical processes will be an important topic for future study.

1 Introduction Resonance Raman spectroscopy of single-walled carbon nanotubes (SWNTs) has been a powerful tool for sample characterization and probing of a broad range of vibrational and electronic behaviours [1]. The special importance held by the radial breathing mode (RBM) in this regard is in large part due to the strong dependence of its frequency on nanotube diameter. Its relatively low frequency ($\sim$100–300 cm^{-1}) also gives it a narrow resonance window, thus reducing the overlap of the resonance responses of different (n,m) species over broad diameter ranges. These two characteristics allow spectroscopic isolation of relatively pure behaviours of single (n,m) species in mixed-chirality samples. As a result, the RBM has played a critical role in developing spectroscopic approaches to identifying (n,m) structures and mapping the chirality dependence of electronic transitions [2–4]. It has also provided a window for understanding the nature of the optical excitations [5–7] and exciton–phonon coupling [8–11].

An equally rich set of behaviours providing complementary information is available through G-band ($\sim$1590 cm^{-1}) studies, which can provide insight into doping processes [12], metallicity of SWNTs that comprise a sample [13], and electron–phonon coupling behaviours linked to transport properties [14] as just a few examples. While G-band intensities and frequencies have allowed study of certain ensemble behaviours, such as monitoring of different chemical and redox processes, many fundamental behaviours and their chirality dependences are masked at this level. Thus, much of the information tied to the G-band response has only been accessible at the single-tube level. In contrast to the RBM, this results from the weak dependence of G-band frequency on SWNT structure, paired with a broad resonance window resulting from its relatively high frequency. The two characteristics together make it nearly impossible to choose an excitation wavelength that suitably isolates the pure spectral behaviour of a single chirality.

Enabling a broader set of G-band studies at the ensemble level is important for addressing a number of issues that are difficult or laborious to probe at the single tube level, such as establishing the generality of specific behaviours across a wide range of structures, or processes requiring measurement of specific resonance behaviours. These difficulties may be overcome by working with ensemble samples that have been highly enriched in single chiralities or specific electronic types. Tremendous progress has been made recently in the ability of separations chemistry to provide just these kinds of samples. Ion-exchange chromatography of SWNTs wrapped in specific DNA sequences is providing a variety of nearly pure semiconducting species [15]. Density gradient-based separations [16, 17] allow separation by metallicity and diameter, and are providing alternative routes to single-chirality samples. Access to these types of samples has allowed new photophysical behaviours that were previously inaccessible to be revealed. Examples include numerous dynamics studies on pure (6,5) samples [18] and probing of dark excitonic states [19, 20].

We demonstrate here examples of how samples enriched in specific types of SWNTs have allowed us to probe behaviours linked to low-energy electron excitations coupled to transport processes and the fundamental nature of the Raman scattering process at resonance with optical excitations, both through observation of G-band spectra. We show that by tuning specific parameters in density-based separations, samples highly enriched in armchair metallic SWNTs are produced. G-band response suggests that a loss of the longitudinal optical (LO) mode is general to all armchairs. Single-chirality semiconducting samples allow us to obtain for the first time full resonance excitation profiles for the G-band. The observed profiles overturn the long-held assumption that intensities are equivalent for response resonant with the incident photon in comparison to the response of the scattered photon resonance.

2 Experimental

2.1 Chirality enrichment Isolation of armchair SWNT species is obtained through density gradient ultracentrifugation (DGU) using a previously-reported approach [21]. Briefly, SWNTs are suspended in 1% aqueous sodium deoxycholate (DOC), with DGU performed in a 3-component mixture of sodium dodecyl sulphate, sodium cholate and DOC. After isolation of the fraction of interest, the sample was dialysed into 1% DOC to provide stable suspension and elimination of the iodixanol density gradient matrix. Enrichment in single-chirality semiconducting species is obtained from ion-exchange chromatography of suspensions of DNA-wrapped SWNTs [15]. For the specific example shown below of the (10,2) species, wrapping in $(TATT)_2TAT$ provides the required selectivity. After chromatographic isolation of the (10,2)-enriched fraction, the sample is dialysed into DOC (1 wt.%) for Raman analysis.

2.2 Raman spectroscopy The wide range of excitation wavelengths used in this study (460–850 nm) was provided from Ti:Sapphire, dye (using Kiton Red and Rhodamine 6G), and frequency-doubled Ti:Sapphire lasers. Raman spectra are obtained in a backscattering configuration with typically 25 mW of incident power. Scattered light is collected, dispersed in a triple-monochromator, and detected on red or green sensitive CCDs with 2–5 min integration times.

3 Results and discussion

3.1 Kohn anomaly in the armchair limit G-band spectra for semiconducting and metallic SWNTs are shown in Fig. 1. The narrow bands in the semiconducting spectrum (weak G^- lower frequency transverse optical (TO) mode, and strong G^+ high frequency LO mode) transform in metallic SWNTs to a broad and more intense G^- relative to the still-narrow G^+. It has been shown both theoretically [14] and experimentally [22–24] that the occurrence of a Kohn anomaly in metallic nanotubes results in significant softening and broadening of the LO mode, so that the G^- and G^+ assignments are reversed from the semiconducting case. Spectra obtained on chirality-identified single tubes indicate the LO broadening is an intrinsic feature of all metallic SWNTs, but its width and intensity relative to the G^+ feature displays a significant chirality dependence [22]. Interestingly, the LO mode was found to be absent at the single tube level for the (15,15) armchair chirality [22], and more recently in the (10,10) structure [25], in agreement with

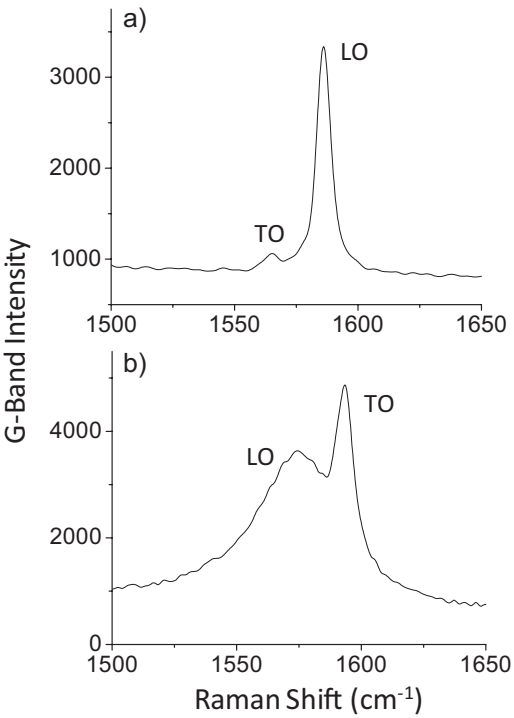

Figure 1 Representative G-band spectra for (a) semiconducting and (b) metallic carbon nanotubes.

the expectation that it is symmetry forbidden for armchair structures. In contrast, recent theory suggests armchair species will still display significant LO mode intensity [26]. It is therefore of interest to determine if its absence is a general feature of all armchair chiralities. The challenge for addressing this question at the ensemble level is to obtain spectra from samples that are highly enriched in armchair species.

Absorption spectra of as-produced SWNT suspensions in 1% aqueous DOC, in comparison to DGU-enriched fractions, are shown in Fig. 2a. The spectrum of the DGU fraction clearly shows elimination of the absorption features originating in the E_{11}, E_{22} and higher-order semiconducting transitions, suggesting a significant degree of enrichment in metallic species. Corresponding photoluminescence spectra (not shown) from the same samples show complete loss of emission from the metallic-enriched sample, indicating significant elimination of the semiconducting species.

While the absorption and photoluminescence spectra demonstrate a high degree of metallic enrichment (~98% [21]), the details of the final chirality distribution in this fraction can only be provided through its extensive Raman characterization. Raman spectra of the RBM region for the as-produced and metallic-enriched fractions are shown in Figs. 2b and c. The spectra were obtained with excitations at 655 and 500 nm, respectively; near the E_{11} resonance peaks for the (10,10) and (7,7) species. The spectrum at 655 nm excitation for the as-produced sample is dominated by semiconducting species of the $(2n+m)=19$ and 20 families (Fig. 2b top, black trace). RBM features for the metallic $(2n+m)=30$ family are also present, but relatively weak in comparison. At 500 nm excitation (Fig. 2c top, black trace), semiconducting transitions are avoided, but RBM features from the (8,5) and (9,3) species overlap with the (7,7) response.

A striking difference is observed for the RBM spectra taken of the metallic-enriched fraction. All semiconducting features have been eliminated. Of special note is that, at 655 nm excitation, the (10,10) RBM, previously the weakest feature in the as-produced spectrum, is now the dominant feature (Fig. 2b, bottom, red trace). Likewise, we observe with 500 nm excitation (Fig. 2c bottom, red trace) that the (7,7) RBM becomes the dominant feature, with only weak contribution from the (8,5) also appearing.

This behaviour is found to be general for all the metallic $2n+m$ families. From the relatively large $2n+m=33$ family to the smallest diameters $(2n+m=18)$, the RBM feature of the armchair goes from being the weakest RBM spectral feature in the as-produced sample to the strongest feature in the enriched spectra. The RBM data demonstrate the interesting result that not only does the DGU process enrich the final sample in metallic nanotubes, but also that the enrichment is selective towards the armchair species.

The ability to spectrally isolate the armchair species allows us to obtain a pure G-band spectrum for these chiralities. In Fig. 3 are shown the corresponding G-band spectra for excitations at 500 and 655 nm, obtained from the as-produced and metallic-enriched samples. With excitation

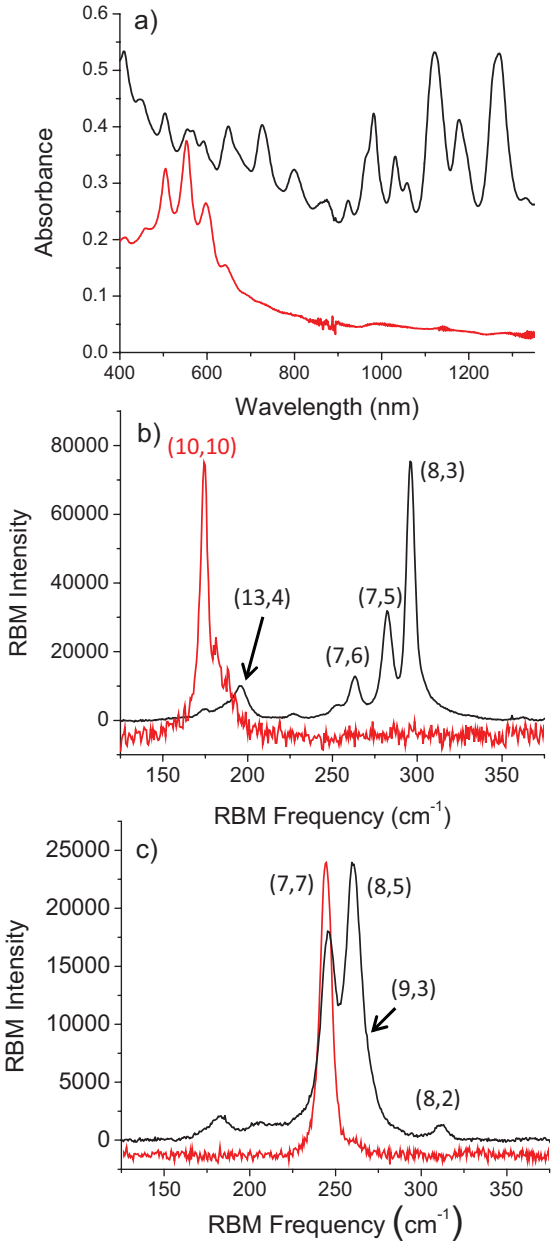

Figure 2 (online colour at: www.pss-b.com) (a) Absorption spectra of as-produced HiPco nanotube suspension (upper, black trace) and metallic-enriched fraction (lower, red trace). (b) RBM spectra of as-produced nanotube suspension (upper, black trace) and metallic-enriched (lower, red trace) fraction at 655 nm excitation and (c) at 500 nm excitation.

at 500 nm, the broad G^- feature expected for metallic nanotubes is clearly present at 1525 cm^{-1} in the as-produced sample (Fig. 3a top, black trace). However, the G-band spectrum of the armchair-enriched sample (Fig. 3a bottom, red trace) shows a single sharp G^+ band at 1590 cm^{-1}. The RBM spectrum of Fig. 2c clearly shows that at 500 nm excitation resonance is with solely the (7,7) chirality. The result of Fig. 3a thus indicates that the broad LO feature has been eliminated in the (7,7) structure.

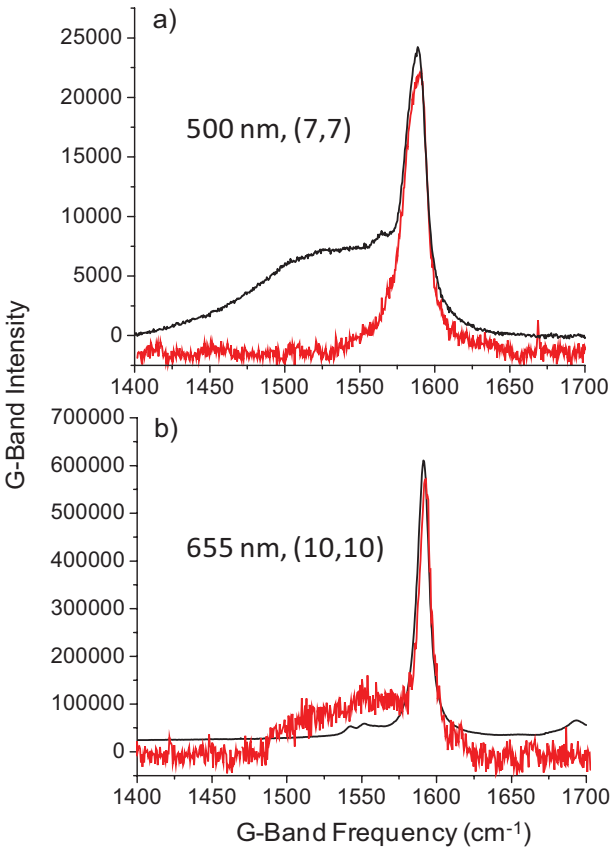

Figure 3 (online colour at: www.pss-b.com) (a) G-band spectra of as-produced nanotube suspension (upper, black trace) and metallic-enriched (lower, red trace) fraction at 500 nm excitation and (b) at 655 nm excitation.

A similar result is found for 655 nm excitation, which as indicated in Fig. 2b should be selective for the (10,10) chirality in the armchair-enriched sample. The G-band spectrum obtained at this wavelength in the as-produced sample (Fig. 3b top, black trace) reflects the large response expected from the semiconducting species that are present in the unseparated sample. Upon removal of the semiconducting species with the armchair enrichment, however, we are left with a G-band spectrum that is primarily a single sharp G^+ feature. The broad residual G^- response likely occurs from the small degree of non-armchair metallics that remain from the $2n+m=30$ family after separation. These are apparent as the shoulders at higher frequency from the (10,10) peak in the armchair-enriched RBM spectrum (Fig. 2b, red trace) that correspond to the (11,8) and (12,6) structures. Loss of the LO mode for the larger diameter (10,10) is therefore also indicated, in agreement with the results of Ref. [25].

Obtaining this result at the ensemble level is suggestive that the loss of intensity in the LO mode in armchair chiralities is a general result for all armchairs. While this must be further demonstrated by obtaining similarly pure G-band spectra for other armchair species, the expectation from symmetry arguments that the LO mode should be absent in armchair structures is confirmed. This result has important implications for understanding and engineering of electron scattering behaviour in transport applications. Because of its strong electron–phonon coupling, the LO mode has been shown to be a significant source of electron scattering in transport processes [27]. As a result, large non-equilibrium populations of G-band excited vibrational states are observed in devices under source-drain bias [28]. The LO mode's absence in armchair structures suggests that this source of scattering may be eliminated, implying that armchairs may be attractive components for interconnects.

3.2 Non-Condon effects in the G-band resonance window The common models used in understanding Raman scattering from SWNTs originate in the Kramers–Heisenberg formalism for the polarizability. The inherent problem of accounting for the sum over states in the electronic overlap terms has been solved through incorporating expressions for density of states [29] and introducing many-body effects to account for the excitonic nature of the optical excitations. The result is a commonly used expression that describes the bandshape of the Raman excitation profile [30]:

$$I \propto \left| \frac{M}{\left(i(E_{ii}-E_{\text{laser}})+\Gamma\right)\left(i(E_{ii}-E_{\text{laser}}-E_{\text{phonon}})+\Gamma\right)} \right|^2 . \quad (1)$$

In Eq. (1), M includes the matrix elements for exciton–phonon and exciton–photon coupling, E_{ii} is the energy of the resonant electronic transition, E_{laser} is the excitation energy, E_{phonon} is the energy of the mode being probed in the Raman measurement and Γ is a phenomenological damping factor that defines the transition width. The resulting profile gives two peaks corresponding to resonances with the incident and scattered photons. The underlying assumption in Eq. (1) is that the two resonances have equivalent intensities.

This formula has been proven successful in the analysis of excitation profiles of the RBM and has also been assumed to be appropriate for other modes as well. However, the validity of this model has not been tested under conditions in which the two resonances can be sufficiently resolved to confirm the assumption of equal contributions. Sufficient separation of the resonances requires probing of a relatively high frequency mode like the G-band. To avoid overlapping spectral contributions to the G-band profile from multiple chiralities, however, requires measurement of samples highly enriched in a single chirality, such as the single-chirality semiconducting fractions made available from ion-exchange chromatography of DNA-wrapped SWNTs [15].

As an example, we show in Fig. 4a the absorption spectrum for a fraction that has been highly-enriched in the (10,2) chirality. The spectrum is dominated by the features corresponding to the E_{11} (at 1061 nm) and E_{22} transitions (at 740 nm). Minor features at 907 and 656 nm correspond to the respective phonon sidebands of the two transitions, with only

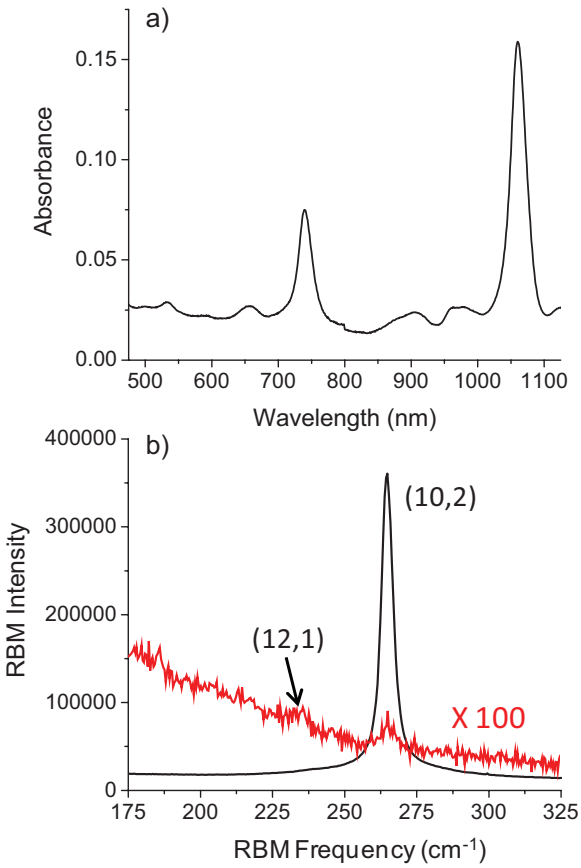

Figure 4 (online colour at: www.pss-b.com) (a) Absorption spectrum of (10,2) enriched sample. (b) RBM spectra of the (10,2) enriched sample with excitation on resonance at 730 nm (black trace) and off-resonance at 800 nm (red trace).

minor additional features being observed from impurity species. Likewise, the RBM spectrum obtained with excitation near resonance with the E_{22} transition (730 nm, Fig. 4b black trace) shows a single Lorentzian feature at 265 cm^{-1}, indicating the extremely high enrichment in (10,2). Minor presence of other semiconducting species is evident in RBM spectra taken at resonance with other semiconducting families. But, as seen in the spectrum taken at resonance with the $2n+m=25$ E_{22} transitions (800 nm, Fig. 4b red trace), intensities for these species are $<1\%$ of that found for the (10,2) structure.

The high degree of enrichment in this sample allows the acquisition of G-band spectra corresponding to the pure behaviour of the (10,2) chirality. A plot of the (10,2) G^+ intensity as excitation energy is varied is shown in Fig. 5. Remarkably, we find a clear asymmetry in the excitation profile. The scattered resonance peak at 1.86 eV is seen to be significantly weaker than the incident resonance at 1.67 eV. Overlaid on the experimental data (black dashed line) is the expectation for the shape of the resonance window based on the exciton description of Eq. (1), which clearly fails. In contrast, we find that the resonance lineshape can be well-fit

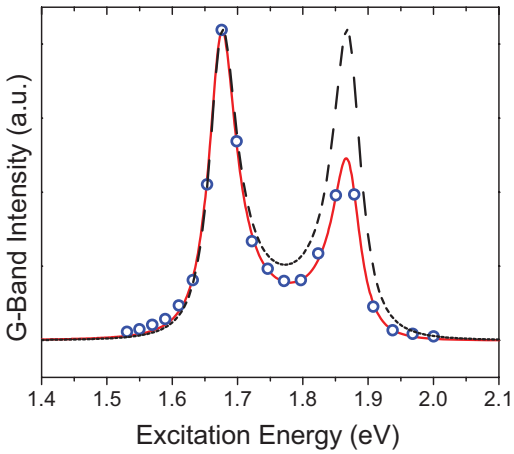

Figure 5 (online colour at: www.pss-b.com) Plot of (10,2) G^+ intensity as a function of excitation energy (blue circles) with a fit to the data using the four-level model of Eq. (2) (red solid line) and an overlay of the corresponding expectation for the exciton model of Eq. (1) (black dashed line).

by invoking a four-level model for resonance Raman scattering described in Eq. (2) [31]:

$$I \propto \left| \frac{\mu_1}{(i(E_{ii}-E_{\text{laser}})+\Gamma)} + \frac{\mu_2}{(i(E_{ii}-E_{\text{laser}}-E_{\text{phonon}})+\Gamma)} \right|^2 . \quad (2)$$

In Eq. (2), μ_1 and μ_2 now represent the matrix elements for the incident and scattered resonant processes, respectively. The four-level model is appropriate in the case of resonance with discrete electronic and vibrational levels such as in molecular systems. Such a description works well for SWNTs both as a result of the discrete nature of the excitonic transitions and the presence of the van Hove singularities in the one-dimensional (1D) density of states. Furthermore, momentum conservation for photon and phonon absorption and emission limits optical activity to the zone centre.

The four-level fit accurately reproduces the E_{22} value obtained from the absorption spectrum (1.67 eV). Furthermore, the fit results from identical values of gamma (26 meV) being incorporated for both resonances, indicating that the difference in their intensities does not originate from variability in the broadening mechanisms for each term. We find the ratio of the matrix elements (μ_2/μ_1) to be -0.75. It is noteworthy that a best fit requires the two matrix elements to have opposite sign.

The origins of this strong asymmetry between the two resonances can be understood as the result of violation of the Condon approximation, which assumes no nuclear motion during an electronic excitation. Such non-Condon effects are generalized here as the introduction of a strong nuclear coordinate dependence in the transition moment dipole for the accompanying absorption and emission processes. Behaviour similar to that in Fig. 5 is commonly observed

in metalloporphyrins, for which such non-Condon effects are significant [32]. The importance of non-Condon behaviour for SWNT optical processes has been suggested previously through analysis of RBM overtone excitation behaviour [10]. Violation of the Condon approximation in SWNTs, in combination with recent observations of breakdown of the adiabatic Born–Oppenheimer approximation in single metallic nanotubes [33], demonstrates the ability of these unique 1D systems to continue to challenge our understanding of their quantum behaviours.

4 Conclusions The ability to eliminate the spectral congestion arising from the overlap of features from multiple chiralities in samples highly enriched in a single (n,m) species is creating the opportunity to reveal new unexplored electronic behaviours in SWNTs. We have shown here the importance of accessing such pure spectral behaviours for providing additional understanding of electron–phonon coupling processes in metallic SWNTS through observation of the absence of the LO mode in armchair structures. Additionally, we have also shown that the long-held assumption of equivalent resonance behaviours in coupling to incident and scattered photons must be re-evaluated. The result calls for a reassessment of how we view the Raman scattering process in SWNTs and raises new questions to explore, including what are the origins of the non-Condon behaviour and what consequences does it hold for other optical processes in SWNTs.

Acknowledgements JGD acknowledges the support of a LANL-LDRD Directors Postdoctoral Fellowship. AKS acknowledges the support of NSF grant DMR 0706574. JK and EHH were supported by the DOE/BES (through Grant No. DE-FG02-06ER46308), the Robert A. Welch Foundation (through Grant No. C-1509), and the Air Force Research Laboratories (through Contract No. FA8650-05-D-5807). This work was performed in part at the Center for Integrated Nanotechnologies, a U.S. Department of Energy, Office of Basic Energy Sciences user facility.

References

[1] M. S. Dresselhaus, A. Jorio, M. Hofmann, G. Dresselhaus, and R. Saito, Nano Lett. **10**, 751 (2010).
[2] S. K. Doorn, D. A. Heller, P. W. Barone, M. L. Usrey, and M. S. Strano, Appl. Phys. A **78**, 1147 (2004).
[3] H. Telg, J. Maultzsch, S. Reich, F. Hennrich, and C. Thomsen, Phys. Rev. Lett. **93**, 177401 (2004).
[4] C. Fantini, A. Jorio, M. Souza, M. S. Strano, M. S. Dresselhaus, and M. A. Pimenta, Phys. Rev. Lett. **93**, 14706 (2004).
[5] P. T. Araujo, S. K. Doorn, S. Kilina, S. Tretiak, E. Einarsson, S. Maruyama, H. Chacham, M. A. Pimenta, and A. Jorio, Phys. Rev. Lett. **98**, 067401 (2007).
[6] E. H. Haroz, S. Bachilo, R. B. Weisman, and S. K. Doorn, Phys. Rev. B **77**, 125405 (2008).
[7] S. K. Doorn, P. T. Araujo, K. Hata, and A. Jorio, Phys. Rev. B **78**, 165408 (2008).
[8] M. Machon, S. Reich, H. Telg, J. Maultzsch, P. Ordejon, and C. Thomsen, Phys. Rev. B **71**, 035416 (2005).
[9] S. V. Goupalov, B. C. Satishkumar, and S. K. Doorn, Phys. Rev. B **73**, 115401 (2006).
[10] A. P. Shreve, E. H. Haroz, S. M. Bachilo, R. B. Weisman, S. Tretiak, S. Kilina, and S. K. Doorn, Phys. Rev. Lett. **98**, 037405 (2007).
[11] Y. Yin, A. N. Vamivakas, A. G. Walsh, S. B. Cronin, M. S. Unlu, B. B. Goldberg, and A. K. Swan, Phys. Rev. Lett. **98**, 037404 (2007).
[12] L. Kavan, P. Rapta, L. Dunsch, M. J. Bronikowski, P. Willis, and R. E. Smalley, J. Phys. Chem. B **105**, 10764 (2001).
[13] S. D. M. Brown, A. Jorio, P. Corio, M. S. Dresselhaus, G. Dresselhaus, R. Saito, and K. Kneipp, Phys. Rev. B **63**, 155414 (2001).
[14] M. Lazzeri, S. Piscanec, F. Mauri, A. C. Ferrari, and J. Robertson, Phys. Rev. B **73**, 155426 (2006).
[15] X. Tu, S. Manohar, A. Jogota, and M. Zheng, Nature **460**, 251 (2009).
[16] M. S. Arnold, S. I. Stupp, and M. C. Hersam, Nano Lett. **5**, 713 (2005).
[17] M. S. Arnold, A. A. Green, J. F. Hulvat, S. I. Stupp, and M. C. Hersam, Nature Nanotechnol. **1**, 60 (2006).
[18] L. Luer, S. Hoseinkhani, D. Polli, J. Crochet, T. Hertel, and G. Lanzani, Nature Phys. **5**, 54 (2009).
[19] O. N. Torrens, M. Zheng, and J. M. Kikkawa, Phys. Rev. Lett. **101**, 157401 (2008).
[20] Y. Murakami, B. Lu, S. Kazaoui, N. Minami, T. Okubo, and S. Maruyama, Phys. Rev. B **79**, 195407 (2009).
[21] E. H. Haroz, W. D. Rice, B. Y. Lu, S. Ghosh, R. H. Hauge, R. B. Weisman, S. K. Doorn, and J. Kono, ACS Nano **4**, 1955 (2010).
[22] Y. Wu, J. Maultzsch, E. Knoesel, B. Chandra, M. Huang, M. Y. Sfeir, L. E. Brus, J. Hone, and T. F. Heinz, Phys. Rev. Lett. **99**, 027402 (2007).
[23] K. T. Nguyen, A. Gaur, and M. Shim, Phys. Rev. Lett. **98**, 145504 (2007).
[24] M. Fouquet, H. Telg, J. Maultzsch, Y. Wu, B. Chandra, J. Hone, T. Heinz, and C. Thomsen, Phys. Rev. Lett. **102**, 075501 (2009).
[25] T. Michel, M. Paillet, D. Nakabayashi, M. Picher, V. Jourdain, J. C. Meyer, A. A. Zahab, and J.-L. Sauvajol, Phys. Rev. B **80**, 245416 (2009).
[26] J. S. Park, K. Sasaki, R. Saito, W. Izumida, M. Kalbac, H. Farhat, G. Dresselhaus, and M. S. Dresselhaus, Phys. Rev. B **80**, 081402(R) (2009).
[27] V. Perebeinos, J. Tersoff, and P. Avouris, Phys. Rev. Lett. **94**, 086802 (2005).
[28] M. Oron-Carl and R. Krupke, Phys. Rev. Lett. **100**, 127401 (2008).
[29] M. Cardona and G. Guntherodt (eds.), Light Scattering in Solids II, Topics in Applied Physics, Vol. 50 (Springer, Heidelberg, 1982), chap. 2.
[30] A. N. Vamivakas, A. Walsh, Y. Yin, M. S. Unlu, B. B. Goldberg, and A. K. Swan, Phys. Rev. B **74**, 205405 (2006).
[31] J. Tang and A. C. Albrecht, in: Raman Spectroscopy: Theory and Practice, Vol. 2 (Plenum, New York, 1970), pp. 33–68.
[32] R. Kumble, T. S. Rush, III, M. E. Blackwood, Jr., P. M. Kozlowski, and T. G. Spiro, J. Phys. Chem. B **102**, 7280 (1998).
[33] A. M. Bushmaker, V. V. Deshpande, S. Hsieh, M. W. Bockrath, and S. B. Cronin, Nano Lett. **9**, 607 (2009).